RHEOLOGICAL BEHAVIOR OF AQUEOUS SUSPENSIONS OF HIGHLY-REFINED PULP FIBRES

Antti Koponen[1], Juan Cecchini[2], Marjo Järvinen[1] and Olli-Ville Laukkanen[1]

[1]VTT Technical Research Centre of Finland Ltd, Koivurannantie 1, 40400 Jyväskylä
[2]Valmet Technologies, Inc., Rautpohjankatu 3, 40700 Jyväskylä, Finland

ABSTRACT

This study focuses on the rheological properties of highly-refined pulp fibres (HRF) as a potential alternative to energy-intensive microfibrillated and nanofibrillated celluloses (MFC/NFC). HRF, produced via conventional refining, has a broad size distribution but may offer similar functional benefits. We performed a detailed rheological analysis of HRF suspensions at four refining levels and five solids contents (1.2–3.0 wt%), using amplitude and frequency sweep measurements to assess viscoelastic properties, and steady-state viscosity measurements to examine flow behaviour.

INTRODUCTION

Microfibrillated and nanofibrillated celluloses (MFC and NFC) have been researched as additives in papermaking e.g. for improved barrier, strength, surface, and optical properties. The production of MFC and NFC through mechanical fibrillation of pulp fibres requires a significant amount of energy. Therefore, producing fibrous materials containing MFC through extensive refining with a conventional refiner can be a more efficient alternative. This approach has the advantage that it is well-established and readily available on an industrial scale. However, unlike MFC suspensions, this material has a very broad size distribution, as it consists of a mixture of fibrillated fibres and fine particles that form simultaneously during refining. These highly refined pulp fibres (HRF) could replace MFC in a variety of applications. Another promising strategy is to use them directly for novel cellulose-based applications. However, there is currently little information available on the rheological behaviour of the aqueous suspensions of these materials.

In this work, we performed a comprehensive rheological analysis for suspensions of highly-refined fibres at four refining levels and five solids contents ranging from 1.2 to 3.0 wt%. Our rheological characterization included amplitude and frequency sweep measurements to analyze the viscoelastic behaviour of these materials, as well as steady-state viscosity measurements to study the flow behaviour of these materials at various shear rates.

MATERIALS AND METHODS

Fibres

Eucalyptus Bleached Hardwood Kraft Pulp (BHKP) suspension was refined at Valmet Technologies to four specific refining energy (SEC) levels: 600 kWh/t, 760 kWh/t, 1400 kWh/t and 2140 kWh/t. We call these fibre suspensions with an increasing refining level HRF, XFC(a), XFC(b) and MFC. **Fig. 1a** shows the average fibre length and width, and **Fig. 1b** shows the content of A- and B-type fines (flake- and fibril-type elements, respectively) as the function of the specific refining energy for these materials. The solids properties of the fibre suspension were measured using the FS5 Fiber Analyzer (Valmet Automation, Kajaani, Finland). The FS5 measures the fractions optically so that fines A is calculated as a percentage of the projection area of particles, and fines B is calculated as a percentage of particle length. Thus, the values are not directly comparable and do not add up to 100%. For HRF, XFC(a), and XFC(b), the mass concentrations (w/w) used in the measurements were 1.2%, 1.8%, 2.1%, 2.4%, and 3.0%. For MFC, measurements were performed at a single concentration of 2.1%. All suspensions were prepared using tap water with a salinity of 20–50 mg/L.

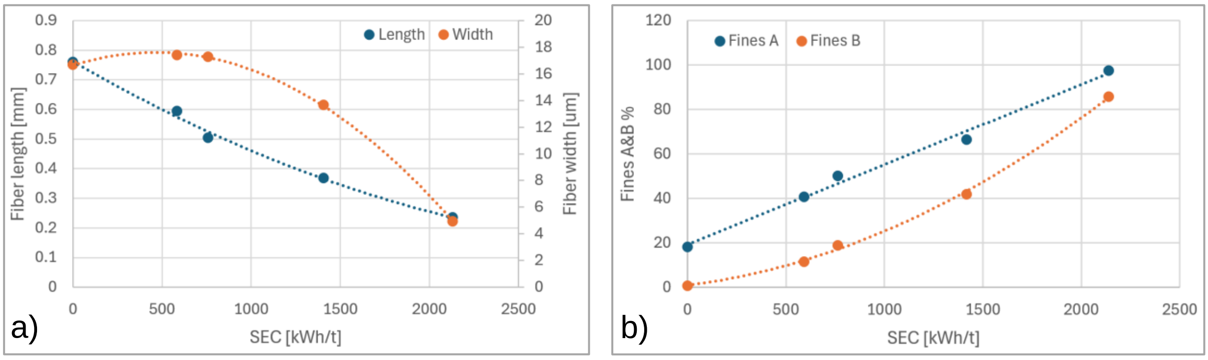

FIGURE 1: a) The fibre length and width as a function of specific refining energy. b) The mass content of A- and B-type fines (flake- and fibril-type elements, respectively) as a function of specific refining energy. Solid lines are included as a guide for the eye.

Rheological measurements

The rheological measurements were performed using a stress-controlled TA Instruments DHR-2 rheometer (**Fig. 2a**) using a wide-gap vane-in-cup geometry (**Fig. 2b**). The cup with a serrated surface was 3D-printed to eliminate wall slip. The diameter of the four-blade vane was 15 mm, and the inner diameter of the transparent cup was 30 mm, resulting in an effective measurement gap of 7.5 mm. The vane geometry was positioned vertically in the middle of the cup – the lower edge of the vane located 16 mm above the bottom of the cup, and the upper edge of the vane located 16 mm below the upper surface of the sample – to avoid end effects. The use of such a wide-gap vane geometry further minimizes possible wall slip effects[1] and avoids confinement effects that would be caused by the large size of the flocs compared to the measurement gap[2]. Notice that the small-gap approximation, typically applicable for standard rheometer geometries like concentric cylinders or cone-and-plate setups, does not hold for the vane-in-cup geometry. Therefore, the shear rate varies radially within the sample[3], and it is more accurate to refer to the shear rate as an apparent shear rate.

The rheological characterization included amplitude sweep measurements ($\gamma_0 = 0.01$ - 1000 %, $\omega = 1$ rad/s) and frequency sweep measurements ($\omega = 0.1$ - 100 rad/s, $\gamma_0 = 0.1$ %) to analyze the viscoelastic behaviour of these materials, as well as steady-state viscosity measurements to study the flow behaviour of these materials at various shear rates (first increasing the apparent shear rate from 0.001 to 100 s^{-1} and then decreasing it from 100 to 0.001 s^{-1}). All rheological measurements were performed at 22 °C.

FIGURE 2: a) Stress-controlled TA Instruments DHR-2 rheometer.
b) The vane geometry and the 3D-printed serrated cup used in this study.
c) The measurement setup.

RESULTS

Steady-state viscosity measurements

Table 1 presents the viscosity values (obtained from the downward sweep) of the different materials at a shear rate of 1.0 s^{-1}. We see that as expected, viscosity increases with increasing fiber concentration and refining energy. The only exception is 2.1% MFC which has a slightly lower viscosity than 2.1% XFC(b). Overall, at a given concentration, the viscosities do not vary significantly. The difference between the lowest and highest viscosity is less than a factor of two. It is somewhat surprising that the viscosities of refined cellulose fibre suspensions remain relatively unchanged, even as the refining energy increases significantly. **Fig. 3** compares the measured viscosities at different concentrations with the viscosities of various MFC grades[4] and highly refined softwood fibres[5] reported in the literature.

TABLE 1 Viscosity (Pa·s) at a shear rate of 1.0 s^{-1} for different materials and concentrations.

%	HRF	XFC(a)	XFC(b)	MFC
1.2	6.5	7.6	10.4	-
1.8	18.6	19.8	31.6	-
2.1	26.1	36.5	48.2	44.2
2.4	35.8	49	63.1	-
3	71.7	82.4	107.8	-

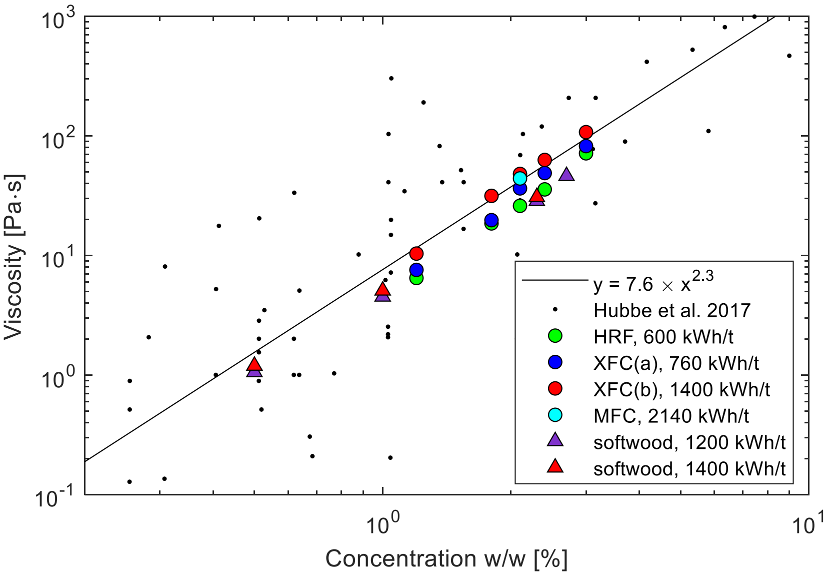

FIGURE 3: Viscosity at a shear rate of 1.0 s^{-1} as a function of concentration for the different materials. Values from a data set for various types of MFC and NFC[4] and highly refined softwood fibres[5] are shown for comparison. The solid line represents a power law fit to the data set from Hubbe et al 2017.

We see from **Fig. 3** that the viscosities of the materials studied here are comparable to the average behaviour of MFCs (see the solid line), with their concentration dependence approximately following a universal[6] power-law relationship. We studied the dependence of the viscosity on the concentration by fitting the power law

$$\eta = Ac^{\alpha} \tag{1}$$

to the data shown in **Table 1**. The values of the fitting parameters, A and α, are shown in **Table 2**. We see that the exponent α is ca. 2.6 for all three materials. This falls well within the range reported in the literature; it is only slightly higher than in the dataset compiled by Hubbe et al.[4]

TABLE 2 Fitting parameter values from Eq. (1) for the different materials. In all cases, R² was greater than 0.98.

	HRF	XFC(a)	XFC(b)
A [Pa·s]	4.00	4.62	6.79
α	2.57	2.66	2.56

Fig. 4 shows shear stress as a function of shear rate, while **Fig. 5** presents viscosity versus shear rate for fibre concentrations of 1.2%, 2.1%, and 3.0%, across the different materials measured both at increasing and decreasing shear rate. The curves are noisier with the two lower refining levels. This is due to the higher inhomogeneity of HRF and XFC(a) when compared to XFC(b) and MFC. With a given shear rate, shear stress and viscosity increase in most cases with increasing refining levels. An exception is 2.1% XFC(b), which exhibits slightly higher stress/viscosity than 2.1% MFC. This could be due to a minor deviation in suspension concentration. However, this difference could also arise from XFB(b) having an optimal combination of short and long fibres that enhances momentum transfer across the material. At the smallest shear rates of an upward sweep, stress initially increases rapidly and then decreases as the shear rate increases. This behaviour occurs because the measurement was started without pre-shearing, resulting in a non-homogeneous structure where the fibres are more flocculated.

Moreover, the data measured at increasing shear rates may be affected by shear banding, particularly at low to intermediate shear rates[7].

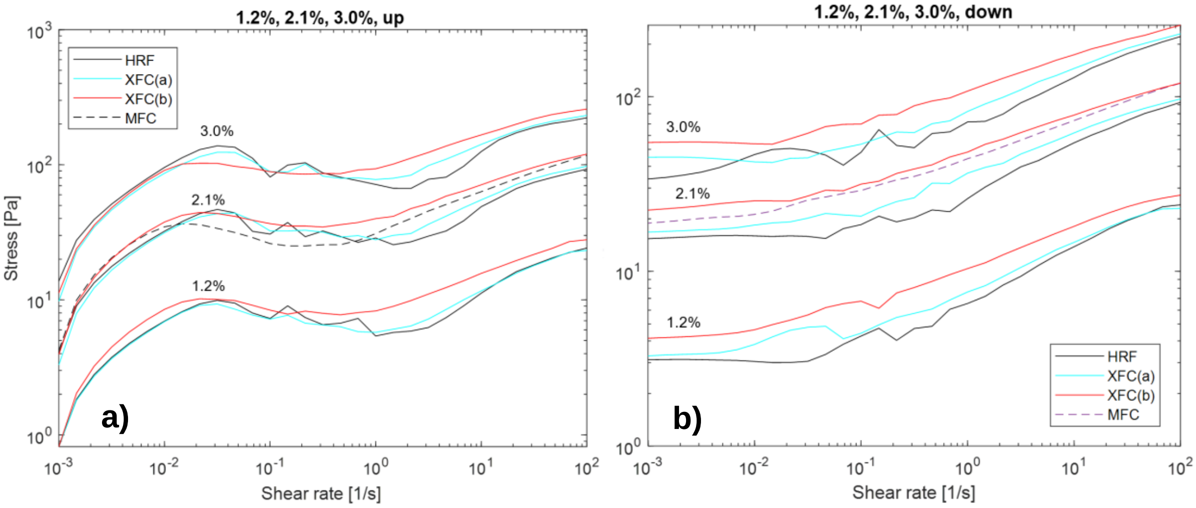

FIGURE 4: Shear stress as a function of shear rate for consistencies 1.2%, 2.1% and 3.0% for the different materials. a) Increasing shear rate. b) Decreasing shear rate.

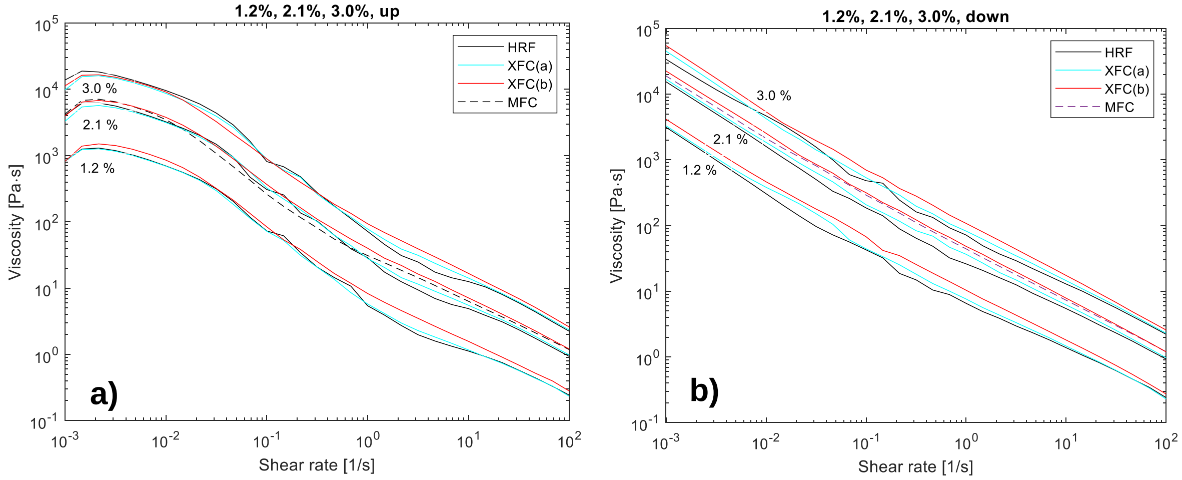

FIGURE 5: Viscosity as a function of shear rate for fibre concentrations 1.2%, 2.1% and 3.0% for the different materials. a) Increasing shear rate. b) Decreasing shear rate.

The stress vs. shear rate curves of the downward sweeps resemble that of a typical Herschel-Bulkley fluid behaviour, namely

$$\sigma = \sigma_0 + K\dot{\gamma}^n \,, \tag{2}$$

where σ is the shear stress, σ_0 the yield stress, K is the consistency index, and n is the flow index. The materials thus exhibit yield stress, and their viscous behaviour approximately follows a power law at high shear rates. We fitted Eq. (2) to the shear stress vs. shear rate curves; an example of a fit is shown in **Fig. 6**. The fitting parameters are provided in **Table 3**. The values of the flow indexes are typical for MFC-type materials at these mass concentrations[6]. Yield stress was similar for all materials with a given concentration. Notice that generally, the measured curves were flat at low shear rates, while the Herschel-Bulkley model fits slightly underestimated the yield stress, as also shown in **Fig. 6.**

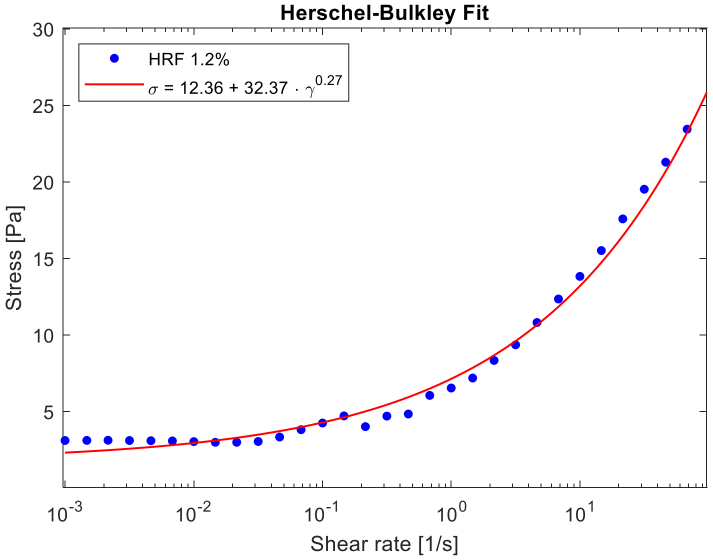

FIGURE 6: Herschel–Bulkley fit, Eq. (2), to the 1.2% HRF flow sweep data with decreasing shear rate.

We studied the dependence of the yield stress on the concentration by fitting the power law

$$\sigma_0 = Bc^{\beta} \tag{3}$$

to the yield stress data shown in **Table 3**. The obtained values for the fitting parameters are shown in **Table 4**. In all cases, the value of parameter β was close to three, which is somewhat higher than typically found in the literature. In the review of Koponen[6], e.g., the mean value of β for various MFC types of materials was 2.3.

TABLE 3: Fitting parameter values from Eq. (2) for the different materials and concentrations. The parameters are consistency index K, flow index n, and yield stress σ_0. R^2 was always greater than 0.97.

	HRF			XFC(a)			XFC(b)			MFC		
[%]	K [Pa s^n]	n [-]	σ_0 [Pa]	K [Pa s^n]	n [-]	σ_0 [Pa]	K [Pa s^n]	n [-]	σ_0 [Pa]	K [Pa s^n]	n [-]	σ_0 [Pa]
1.2	5.4	0.33	1.8	6.3	0.28	1.9	9.1	0.24	1.7	-	-	-
1.8	12.5	0.34	6.7	14.6	0.32	7.2	23.7	0.25	8.6	-	-	-
2.1	18.5	0.34	11.1	26.6	0.27	10.2	36.3	0.24	13.0	32.4	0.27	12.4
2.4	22.7	0.35	17.4	36.2	0.27	15.0	49.3	0.22	15.5	-	-	-
3.0	43.4	0.33	31.2	57.7	0.28	28.2	80.8	0.23	29.5	-	-	-

TABLE 4 Fitting parameter values from Eq. (3) for the different materials. In all cases, R^2 was greater than 0.98.

	HRF	XFC(a)	XFC(b)
B [Pa]	1.03	1.19	1.14
β	3.17	2.91	3.07

Amplitude sweep measurements

Figs. 7 and **8** show the storage modulus and the loss modulus as functions of strain amplitude, respectively. The shapes of the curves are typical for MFC-type materials[8]. In the linear viscoelastic regime (strain amplitude < 1%), G’ generally increases with increasing refining levels. An exception is 3.0% HRF which has higher G’ and G’’ than XFC(a) in this regime. With strain amplitude > 10% this anomaly vanishes. To check whether this was due to slight variations in concentration, we repeated the measurements and obtained the same result. Then, by gradually decreasing the concentration, we found that at concentrations below 2.7%, XFC(a) exhibited higher G′ and G″ values than HRF. At present, we do not have an explanation for this behaviour.

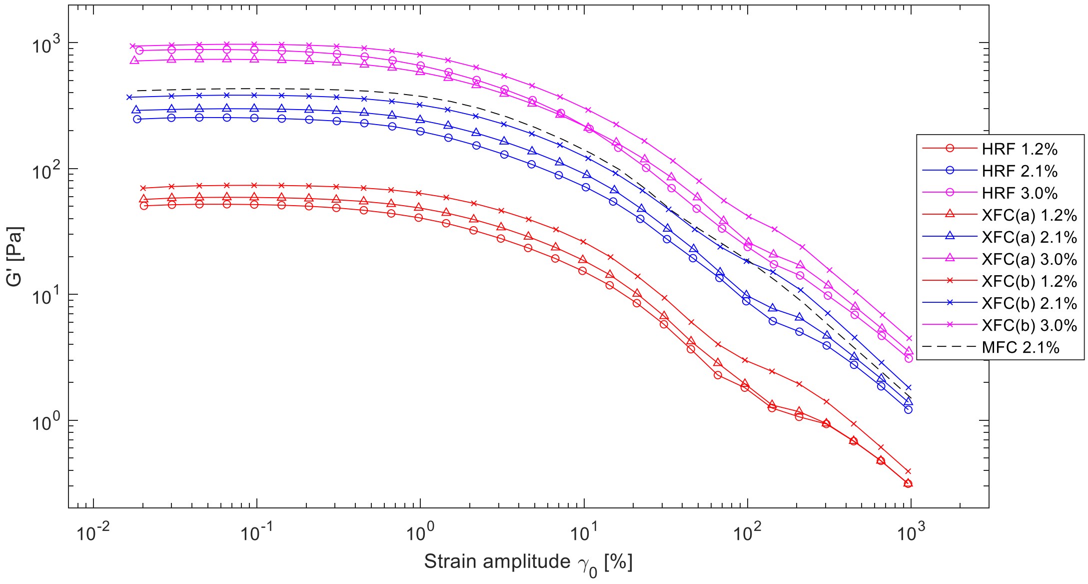

FIGURE 7: Storage modulus G’ as a function of strain amplitude for the different materials and concentrations of 1.2%, 2.1% and 3.0%.

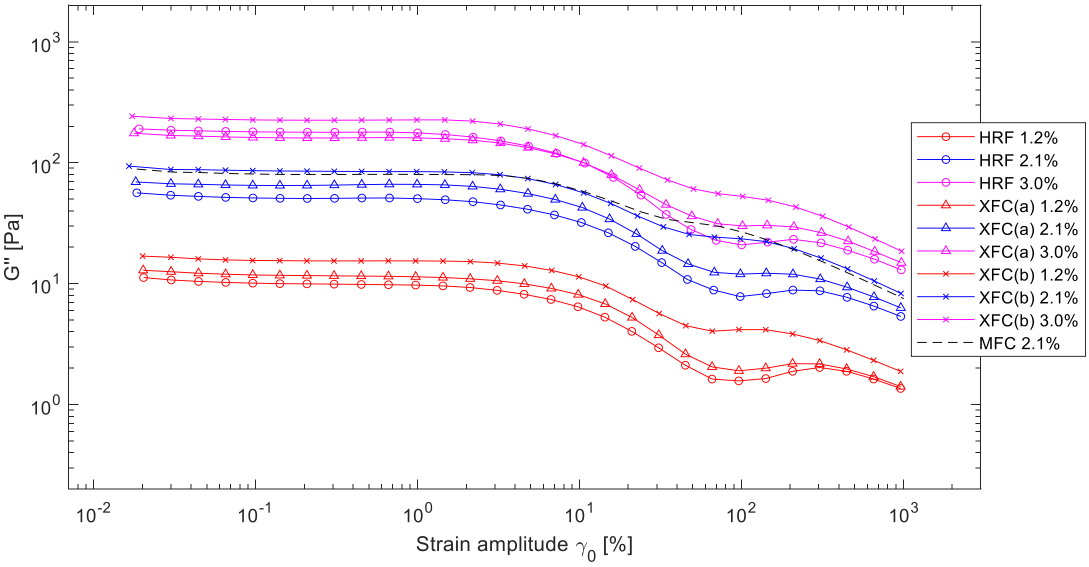

FIGURE 8: Loss modulus G’’ as a function of strain amplitude for the different materials and concentrations 1.2%, 2.1% and 3.0%.

We determined the values of the storage and loss modulus in the linear viscoelastic (LVE) region. The LVE region was defined as the strain range over which G′ and G’’ remained approximately constant, indicating undisturbed material structure. The onset of nonlinearity was identified as the point where G′ or G’’ deviated by more than 5% from its initial plateau value. The storage and loss moduli, representative of the LVE region, were calculated as the averages of G′ and G″ within this linear range. **Table 5** shows these values for different materials and concentrations. In **Fig. 9**, G’ and G’’ are presented as a function of concentration. We see from **Fig. 9** that the relation between G’ and G’’ and concentration is a power law

$$G' \text{or } G'' = Dc^{\delta} \ . \tag{4}$$

The fits of Eq. (4) to the data are shown in **Fig. 9** with solid lines. The fitting parameters are shown in **Table 6**. The value δ is close to three in all cases. Similar values can be found in the literature for both MFC and NFC [9-12].

TABLE 5: The storage modulus G’ and loss modulus G’’ in the LVE region for the different materials and concentrations.

	HRF		XFC(a)		XFC(b)		MFC	
[%]	G' [Pa]	G" [Pa]	G' [Pa]	G" [Pa]	G' [Pa]	G" [Pa]	G' [Pa]	G" [Pa]
1.2	50.5	10.3	57.2	11.9	71.7	15.8	-	-
1.8	159.4	33.6	183.1	39.4	234.5	55.3	-	-
2.1	247.0	52.1	292.5	66.0	371.8	86.6	421.6	81.7
2.4	387.2	88.4	434.0	100.2	531.1	126.1	-	-
3.0	853.5	181.9	718.1	164.0	943.0	228.3	-	-

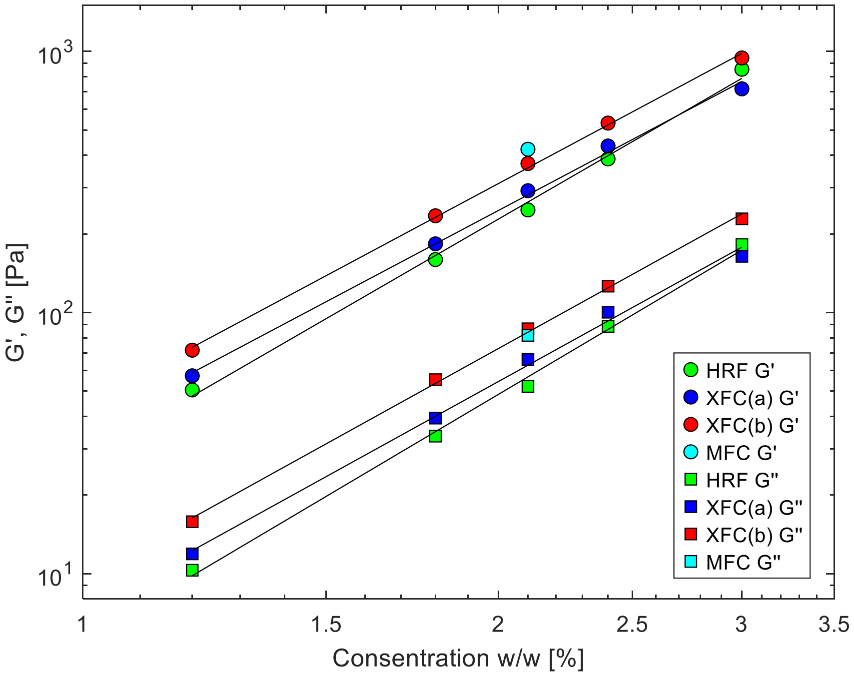

FIGURE 9: Storage modulus and loss modulus in the LVE region as a function of concentration. Solid lines represent power-law fits for each material (excluding MFC).

TABLE 6: Fitting parameter values from Eq. (4) for the different materials.

	HRF G'	HRF G''	XFC(a) G'	XFC(a) G''	XFC(b) G'	XFC(b) G''
D	27.4	5.52	35.3	7.21	43.9	9.58
δ	3.05	3.14	2.80	2.92	2.83	2.93

Frequency sweep measurements

Figs. 10 and **11** show the storage modulus and the loss modulus as functions of angular frequency. All samples can be observed to exhibit strongly elastic behaviour irrespective of the fiber type and concentration, with weak frequency dependence of G' and G''. This is typical behaviour for MFC-type materials[10-12].

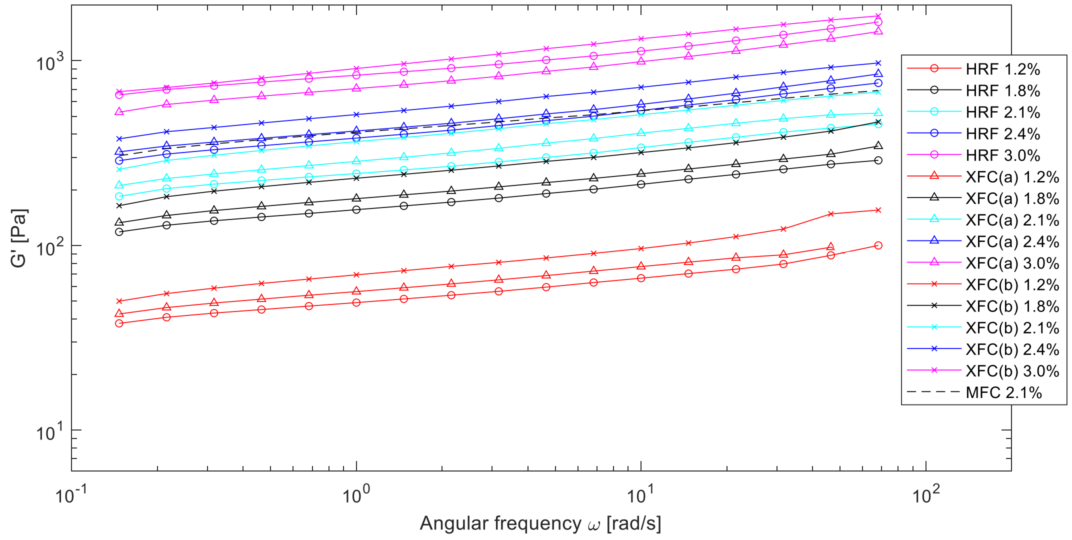

FIGURE 10: Storage modulus G'' as a function of angular frequency for the different materials and concentrations.

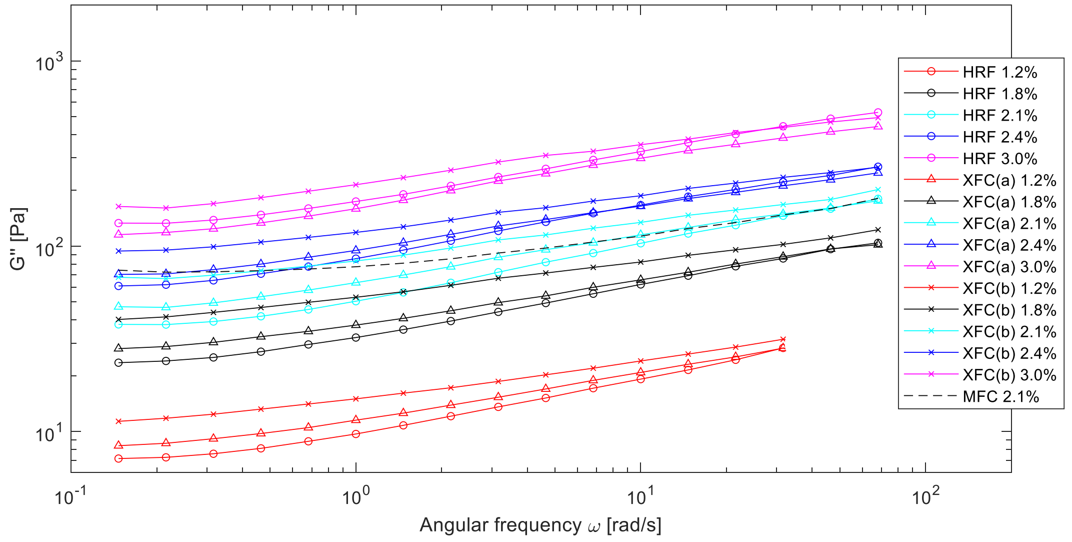

FIGURE 11: Loss modulus G'' as a function of angular frequency for the different materials and concentrations.

SUMMARY

This study provided a comprehensive rheological analysis of highly refined fibres (HRF) as a potential alternative to microfibrillated and nanofibrillated celluloses (MFC/NFC). Four HRF suspensions were studied across a mass concentration range of 1.2% to 3.0%. The results demonstrate that HRF exhibits rheological properties comparable to those of MFC/NFC, despite a broader fibre size distribution. The viscosity of HRF suspensions showed relatively small variation with increasing refining energy, while the yield stress remained nearly constant across all refining levels. The flow, amplitude, and frequency sweeps of the HRF suspensions closely resembled those observed for MFC/NFC. Overall, the findings highlight the potential of HRF as a cost-effective and energy-efficient alternative to MFC/NFC. The ability to produce HRF using conventional refining methods offers a significant advantage for industrial-scale applications, providing a more sustainable approach to enhancing cellulose-based products.

REFERENCES

1. Mohtaschemi, M., Dimic-Misic, K., Puisto, A., Korhonen, M., Maloney, T., Paltakari, J. Alava, M., Rheological characterization of fibrillated cellulose suspensions via bucket vane viscometer, *Cellulose* **2014**, 21, 1305–1312. https://doi.org/10.1007/s10570-014-0235-1.
2. Barnes, H., Nguyen, Q., Rotating vane rheometry—a review, *Journal of Non-Newtonian Fluid Mechanics* **2001**, 98(1), 1–14. https://doi.org/10.1016/S0377-0257(01)00095-7.
3. Chaparian, E., Owens, C., McKinley, G., Computational rheometry of yielding and viscoplastic flow in vane-and-cup rheometer fixtures, *Journal of Non-Newtonian Fluid Mechanics* **2022**, 307, 104857. https://doi.org/10.1016/j.jnnfm.2022.104857.
4. Hubbe, M., Tayeb, P., Joyce, M., Tyagi, P., Kehoe, M., Dimic-Misic, K., Pal, L., Rheology of nanocellulose-rich aqueous suspensions: a review, *Bioresources* **2017**, 12(4), 9556–9661. https://doi.org/10.15376/biores.12.4.Hubbe.
5. Jäsberg, A., Heiskanen, S., Cecchini, J., Kiiskinen, T., Koponen, A., Characterizing rheological behavior and fluidization of highly refined furnishes for process optimization, *TAPPI Journal* **2024**, 23(4), 200-208. https://doi.org/10.32964/TJ23.4.200.
6. Koponen, A., The effect of consistency on the shear rheology of aqueous suspensions of cellulose micro- and nanofibrils: a review, *Cellulose* **2020**, 27(4), 1879-1897. https://doi.org/10.1007/s10570-019-02908-w.
7. Nechyporchuk, O., Naceur Belgacem M., Pignon F., Rheological properties of micro-/nanofibrillated cellulose suspensions: Wall-slip and shear banding phenomena, *Carbohydrate Polymers* **2014**, 112, 432-439. https://doi.org/10.1016/j.carbpol.2014.05.092.
8. Rezayati Charani, P., Dehghani-Firouzabadi, M., E. Afra, E., Shaker, A., Rheological characterization of high concentrated MFC gel from kenaf unbleached pulp, *Cellulose* **2013**, 20, 727–740. https://doi.org/10.1007/s10570-013-9862-1.
9. Schenker, M., Schoelkopf, J., Gane, P., Mangin, P., Influence of shear rheometer measurement systems on the rheological properties of microfibrillated cellulose (MFC) suspensions, *Cellulose* **2018**, 25, 961–976. https://doi.org/10.1007/s10570-017-1642-x.
10. Rezayati Charani, P., Dehghani-Firouzabadi, M., Afra, E., Shakeri, A., Rheological characterization of high concentrated MFC gel from kenaf unbleached pulp. *Cellulose* **2013**, 20, 727–740. https://doi.org/10.1007/s10570-013-9862-1.
11. Agoda-Tandjawa, G., Durand, S., Berot, S., Blassel, C., Gaillard, C., Garnier, C., Doublier, J., Rheological characterization of microfibrillated cellulose suspensions after freezing, *Carbohydrate Polymers* **2010**, 80(3), 677-686. https://doi.org/10.1016/j.carbpol.2009.11.045.
12. Pääkkö, M., Ankerfors, M., Kosonen, H., Nykänen, A., Ahola, S., Österberg, M., Ruokolainen, J., Laine, J., Larsson, P., Ikkala, O., Lindström, T., *Biomacromolecules* **2007** 8(6), 1934-1941. https://doi.org/10.1021/bm061215p.